THE JOURNAL OF BIOLOGICAL CHEMISTRY
Vol. 277, No. 49, Issue of December 6, pp. 47564–47571, 2002

Printed in U.S.A.

Function and Solution Structure of Huwentoxin-IV, a Potent Neuronal Tetrodotoxin (TTX)-sensitive Sodium Channel Antagonist from Chinese Bird Spider *Selenocosmia huwena**

Received for publication, April 25, 2002, and in revised form, August 15, 2002
Published, JBC Papers in Press, September 11, 2002, DOI 10.1074/jbc.M204063200

Kuan Peng, Qin Shu, Zhonghua Liu, and Songping Liang‡

From the College of Life Sciences, Hunan Normal University, Changsha 410081, People's Republic of China

We have isolated a highly potent neurotoxin from the venom of the Chinese bird spider, *Selenocosmia huwena*. This 4.1-kDa toxin, which has been named huwentoxin-IV, contains 35 residues with three disulfide bridges: Cys-2–Cys-17, Cys-9–Cys-24, and Cys-16–Cys-31, assigned by a chemical strategy including partial reduction of the toxin and sequence analysis of the modified intermediates. It specifically inhibits the neuronal tetrodotoxin-sensitive (TTX-S) voltage-gated sodium channel with the IC_{50} value of 30 nM in adult rat dorsal root ganglion neurons, while having no significant effect on the tetrodotoxin-resistant (TTX-R) voltage-gated sodium channel. This toxin seems to be a site I toxin affecting the sodium channel through a mechanism quite similar to that of TTX: it suppresses the peak sodium current without altering the activation or inactivation kinetics. The three-dimensional structure of huwentoxin-IV has been determined by two-dimensional ^{1}H NMR combined with distant geometry and simulated annealing calculation by using 527 nuclear Overhauser effect constraints and 14 dihedral constraints. The resulting structure is composed of a double-stranded antiparallel β-sheet (Leu-22–Ser-25 and Trp-30–Tyr-33) and four turns (Glu-4–Lys-7, Pro-11–Asp-14, Lys-18–Lys-21 and Arg-26–Arg-29) and belongs to the inhibitor cystine knot structural family. After comparison with other toxins purified from the same species, we are convinced that the positively charged residues of loop IV (residues 25–29), especially residue Arg-26, must be crucial to its binding to the neuronal tetrodotoxin-sensitive voltage-gated sodium channel.

Voltage-gated sodium channels play important roles in electrical signaling in almost all kinds of excitable tissues. They are responsible for the generation of action potentials and nervous influx conduction in sensory nerves.

Although the pioneer investigation of tetrodotoxin (TTX)[1] on voltage-gated sodium channels (VGSCs) had been performed by Narahashi *et al.* (1, 2) in 1960s, it was not until early 1990s that people began to classify the voltage-gated sodium channel into two different types (3), tetrodotoxin-sensitive (TTX-S) VGSC and TTX-resistant (TTX-R) VGSC. Further investigations on many other neurotoxins from various biological sources such as ciguatoxin (4), scorpion toxins (5), and μ-conotoxins (6–8) have shown that these toxins can affect VGSCs through quite diverse mechanisms. At least six different sites have been proposed to explain the complicated mechanisms of the targeting VGSCs of these neurotoxins. In short, site I toxins such as TTX and μ-conotoxins bind to an external key site of the pore so that sodium ions can no longer pass the channel. Toxins related to sites II–VI differ greatly from each other as they either affect the activation (β-scorpion toxins) or the deactivation (α-scorpion toxins) of sodium channels, and some of them even exert dual effects on both processes (ciguatoxin) (9).

At the molecular level, the highly glycosylated α-subunit (260 kDa) is responsible for the pore forming of VGSCs. A number of investigations on drug receptor/channel interaction have enabled us to know many key residues for the function of VGSCs. TTX, saxitoxin, and μ-conotoxins have contributed a great deal in probing the structure-function relationship and modulation of variant VGSCs (10–13).

Another potential striking use of VGSC antagonists comes from their implication with pain. VGSCs expressed in primary sensory neurons (dorsal root ganglion (DRG) neurons) are believed to be important targets in the study of the molecular pathophysiology of pain and in the search for new pain therapies (14–16). Peptide toxins with considerable affinity and high selectivity to unique VGSCs are sure to play an important role in this field.

In this study, we focus on the structure-function relationship studies of a highly potent neurotoxin purified from Chinese bird spider, *Selenocosmia huwena*, which is named huwentoxin-IV (HWTX-IV). First, we used patch clamp methods to investigate its effects on VGSCs expressed in adult rat DRG neurons; HWTX-IV selectively inhibits TTX-S VGSCs and shows no significant effect on TTX-R VGSCs. Second, its three-dimensional solution structure was elucidated by using NMR methods; HWTX-IV shares an ancestral global folding pattern with many other neurotoxins called the inhibitor cystine knot (ICK) motif (17). Third, comparison with huwentoxin-I and previously known conotoxins bloking at site I provided us some clues on its toxin-receptor interaction. Besides the disulfide-directed backbone, we think positively

* This work was supported by the National Natural Science Foundation of China (Grants 30170193 and 39990600). The costs of publication of this article were defrayed in part by the payment of page charges. This article must therefore be hereby marked "*advertisement*" in accordance with 18 U.S.C. Section 1734 solely to indicate this fact.

The atomic coordinates and structure factors (code 1MB6) have been deposited in the Protein Data Bank, Research Collaboratory for Structural Bioinformatics, Rutgers University, New Brunswick, NJ (http://www.rcsb.org/).

‡ To whom correspondence should be addressed. Fax: 86-731-886-1304; E-mail: liangsp@public.cs.hn.cn.

[1] The abbreviations used are: TTX, tetrodotoxin; TTX-R, TTX-resistant; TTX-S, TTX-sensitive; DRG, dorsal root ganglion; VGSC, voltage-gated sodium channel; HWTX-IV, huwentoxin IV; ICK, inhibitor cystine knot; Pth, parathyroid hormone; CM, carboxymethyl; R.M.S.D., root mean square difference(s); HPLC, high pressure liquid chromatography; MALDI-TOF MS, matrix-assisted laser desorption/ionization-time of flight mass spectrometry; NOE, nuclear Overhauser effect; NOESY, NOE spectroscopy; DQF, double quantum filtered; TOCSY, two-dimensional total correlation spectroscopy.

charged residues (residue Arg-26 especially) in the extrusive loop IV of the compact molecule must play a crucial role in its targeting TTX-S VGSC.

EXPERIMENTAL PROCEDURES

Toxin Purification and Sequencing—The venom from the female Chinese bird spider (*S. Huwena*) was collected as described in our previous work (18). HWTX-IV was purified by means of ion-exchange and reverse-phase high performance liquid chromatography. Lyophilized crude venom was loaded onto a Waters Protein-Pak CM 8HR ion-exchange column (5 × 50 mm) initially equilibrated with 0.02 M sodium phosphate buffer, pH 6.25 (buffer A). The column was eluted with a linear gradient of 0–50% of buffer B (1 M sodium chloride, 0.02 M sodium phosphate, pH 6.25) over 40 min at a flow rate of 0.7 ml min^{-1}. The fraction of interest was then applied to a Vydac C18 analytical reverse-phase HPLC column (218TP54, 4.6 × 250 mm) and eluted at a flow rate of 0.8 ml min^{-1} using a gradient of 0–20% buffer B (0.1% v/v trifluoroacetic acid in acetonitrile) over 8 min after an equilibrium period of 2 min followed by a gradient of 20–35% buffer B over 40 min. (Buffer A was 0.1% v/v trifluoroacetic acid in water.) Once purified to >95% homogeneity (assessed by reverse-phase HPLC and mass spectrometry), peptide was lyophilized and stored at −20 °C until further use. The molecular mass was determined by matrix-assisted laser desorption/ionization time-of-flight mass spectrometry (MALDI-TOF MS) on a Bruker ProFlex-III mass spectrometer, and the entire amino acid sequence was obtained from a single sequencing run on an Applied Biosystems/PerkinElmer Life Sciences Procise 491-A protein sequencer.

Assignment of the Disulfide Bonds of Huwentoxin-IV by Partial Reduction and Sequence Analysis (19–21)—HWTX-IV (0.1 mg) was solubilized in 10 μl of 0.1 mol/liter citrate buffer (pH 3) containing 6 mol/liter guanidine-HCl. Partial reduction of HWTX-IV disulfide bonds was carried out by adding 10 μl of 0.1 mol/liter Tris (2-carboxyethyl) phosphine at 40 °C for 10 min at pH 3, and the intermediates were isolated by reverse-phase HPLC (column: 218TP54, 4.6 × 250 mm) with linear gradient elution (20~35% acetonitrile in 50 min). The intermediates of partial reduction were collected, and their masses were determined by MALDI-TOF. Appropriate intermediates containing free thiols were dried and then alkalized by adding 100 μl of 0.5 mol/liter iodoacetamide (pH 8.3). The alkalized peptide was desalted by reverse-phase HPLC and then submitted to an Applied Biosystems Model 491 gas-phase sequencer. The Edman degradation was performed with a normal automatic cycle program.

Insect Bioassay—Insect toxicity was determined by intraperitoneal injection of HWTX-IV into the abdomen of adult American cockroaches *Periplaneta americana* at doses of 10–200 μg g^{-1}. Insects were monitored for 48 h after injection.

Cell Isolation Procedures—Rat DRG neurons were acutely dissociated and maintained in short term primary culture using the method described by Hu and Li (22) Briefly, 30-day-old adult Sprague-Dawley rats of either sex were decapitated, and the dorsal root ganglia were isolated quickly from the spinal cord. Then they were transferred into Dulbecco's modified Eagle's medium containing trypsin (0.5 mg ml^{-1}, type III, Sigma), collagenase (1.0 mg ml^{-1}, type IA, Sigma), and DNase (0.1 mg ml^{-1}, type III, Sigma) for incubation at 34 °C for 30 min. Trypsin inhibitor (1.5 mg ml^{-1}, type II-S, Sigma) was used to terminate enzyme treatment. The DRG cells were transferred into 35-mm culture dishes (Corning, Sigma) with the cultured medium (95% Dulbecco's modified Eagle's medium, 5% newborn calf serum, hypoxanthine aminopterin thymidine supplement, and penicillin-streptomycin) and incubated in CO_2 incubator (5% CO_2, 95% air, 37 °C) for 1–4 h before the patch clamp experiment.

Electrophysiological Studies—DRG cells with large diameters (around 50 picosiemens in slow capacitance) and those with relatively small diameters (around 20 picosiemens for slow capacitance) were chosen for study of TTX-S and TTX-R sodium currents, respectively. Meanwhile, TTX (final concentration at 0.2 μM) was used to separate TTX-R sodium current from TTX-S sodium current. Drug-containing solutions of 10-μl volume were applied by pressure injection with a microinjector (IM-5B, Narishige, Tokyo, Japan) through a micropipette (20-μm tip diameter) placed about 100 μm away from the cells under study. Patch clamp experiments were performed at room temperature (20–25 °C) under the whole cell patch clamp configuration. Suction pipettes (2.0–3 microohms) were made of borosilicate glass capillary tubes with a two-step pulling from a vertical micropipette puller (PC-10, Narishige). The pipette solution contained: 145 mM CsCl, 4 mM $MgCl_2 \cdot 6H_2O$, 10 mM HEPES, 10 mM EGTA, 10 mM glucose, 2 mM ATP (the pH was adjusted to 7.2 with KOH). The external solution contained: 145 mM NaCl, 2.5 mM KCl, 1.5 mM $CaCl_2$, 1.2 mM $MgCl_2 \cdot 6H_2O$, 10 mM HEPES, 10 mM glucose (the pH was adjusted to 7.4 with NaOH). Experimental data were collected and analyzed by using the program Pulse/Pulsefit 8.0(HEKA Electronics, Lambrecht/Pfalz, Germany), and macroscopic TTX-S or TTX-R sodium currents were filtered at 10 kHz and digitized at 3 kHz with an EPC-9 patch clamp amplifier (HEKA Electronics, Germany). Series resistance was kept near 5 microohms and compensated 65–70%, and linear capacitative and leakage currents were digitally subtracted by using the P/4 protocol.

NMR Spectroscopy—An NMR sample was prepared by dissolving ~10 mg of HWTX-IV in 500 μl of 20 mM phosphate buffer (H_2O/D_2O, 9/1, v/v) containing 0.002% NaN3 and 0.1 mM EDTA. The pH was adjusted to 4.5 with HCl, and sodium 3-(trimethyl-silyl) propionate-2, 2, 3, 3-D4 was added at a final concentration of 200 μM as an internal chemical shift reference. The final concentration of HWTX-IV was ~5 mM. For experiments in D_2O, the sample used in H_2O experiments was lyophilized and then redissolved in 500 μl of 99.996% D_2O (Cambridge Isotope Laboratories).

All NMR experiments were recorded on a 500 MHz Bruker DMX-500 spectrometer. All two-dimensional spectra were recorded in phase-sensitive mode by the time-proportional phase incrementation method following standard pulse sequences and phase cycling. Solvent suppression was achieved by the presaturation method. Two-dimensional NMR spectra were recorded at a temperature of 300 K, including COSY, DQF-COSY, and TOCSY with a mixing time of 37 and 73 ms, as well as NOESY with a mixing time of 100, 200, and 300 ms. The recording data points of t1 × t2 were 512 × 2048 for COSY and TOCSY, 700 × 4096 for DQF-COSY, and 512 × 2048 for all NOESY spectra except 768 × 4096 for the 100 ms spectrum.

The hydrogen-deuterium exchange experiments were carried out by recording a series of one-dimensional spectra after redissolving the lyophilized H_2O experiment sample in D_2O at time scalar of 10 min, 20 min, 30 min, 1 h, 2 h, 4 h, 6 h, 8 h, and 24 h. A TOCSY spectrum was recorded after 8 h of exchanging.

Spectra were processed and viewed using the software XWINNMR (Bruker) or Felix 98.0 (Biosym Technologies) on the O_2 work station (Silicon Graphics). All data were zero-filled to produce a 2K × 4K real matrix to COSY, DQF-COSY and NOESY or 1K × 2K to TOCSY. Before Fourier transformation, sine bell or sine bell square window functions were used with a phase shift of $\pi/2$.

Structure Calculations—Distance constraints were derived from the intensities of cross-peaks in NOESY spectra with mixing times of 100 or 200 ms. Observed NOE data were classified into strong, medium, and weak, corresponding to upper bound interproton distance restraints of 2.7, 3.5, and 5.0 Å, respectively. Lower distance bounds were taken, and the sum of the van der Waals radii of proton was 1.8 Å. Pseudo-atom corrections were applied to non-stereo measurements specifically assigned to methyl and methylene protons according to the method of Wüthrich (23).

Backbone dihedral constraints were derived from $^3J_{HNH\alpha}$ coupling constants measured from either one-dimensional NMR spectra or the anti-phase cross-peak splitting in a high digital resolution DQF-COSY spectrum. 14 ϕ dihedral angles were restrained to −120 ± 40 (degree) for a $^3J_{HNH\alpha} \geq 8$ Hz and −65 ± 25 (degree) for $^3J_{HNH\alpha} \leq 5.5$ Hz.

HWTX-IV contains 6 cysteine residues paired as Cys-2–Cys-17, Cys-9–Cys-24, and Cys-16–Cys-31, assigned by partial reduction and sequence analysis. Nine additional fake distance constraints were added to define the three disulfide bonds involved in HWTX-IV. For each disulfide bond, three distance constraints, S(i) − S(j), S(i) − C_β(j), and S(j) − Cβ(i), were set to 2.02 ± 0.02, 2.99 ± 0.5, and 2.99 ± 0.5 Å, respectively. Irredundant distance constraints derived from NOEs and dihedral constraints derived from $^3J_{HN\alpha}$ coupling constants have been used to calculate the structure of HWTX-IV by distance geometry and simulated annealing calculation with the program XPLOR (24).

RESULTS

Isolation and Sequencing of HWTX-IV—HWTX-IV was purified by a combined use of ion-exchange HPLC and reverse-phase HPLC as described before (Fig. 1). Its molecular mass is 4107.5 Da, read from its mass spectrometry. The amino acid sequence of HWTX-IV, as shown in Fig. 4, is composed of 35 amino acids residues including six cysteine residues.

Assignment of the Disulfide Bonds of Huwentoxin-IV by Partial Reduction and Sequence Analysis—Fig. 2 shows the HPLC separation of the mixture obtained from the partial reduction

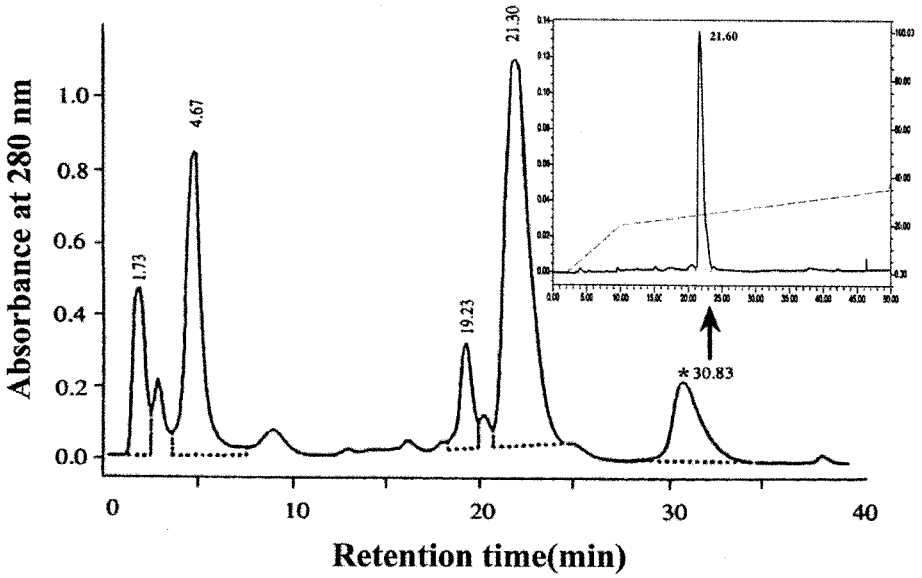

FIG. 1. **Purification of HWTX-IV.** The absorbent peak (retention time as 30.83) labeled with a * symbol in ion-exchange chromatography was further purified with reverse-phase HPLC as shown in the *inset*. The *dashed line* in the *inset* displays the buffer B percentage in the dilution gradient. HWTX-IV is washed out at 24% buffer B.

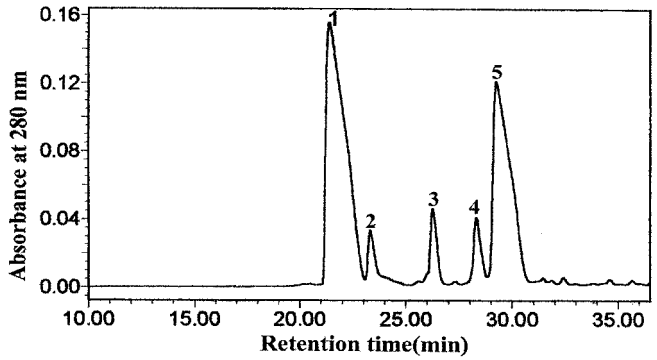

FIG. 2. **Analytical reverse-phase HPLC profile of partial reduction of HWTX-IV by TCEP.** Five chromatographic peaks contain intact peptide and partially reduced intermediates, respectively. The main peak (*peak 1*) represents intact HWTX-IV, whose observed mass is the same as the native oxidized toxin. *Peak 2* with a mass 2 Da greater than that of native HWTX-IV indicates one of the three disulfide bonds possibly reduced. The masses of *peak 3* and *peak 4* are both 4 Da heavier than intact peptide, suggesting that two disulfide bonds are reduced to four free thiol groups. *Peak 5* represents completely reduced peptide with a mass 6 Da heavier than intact HWTX-IV.

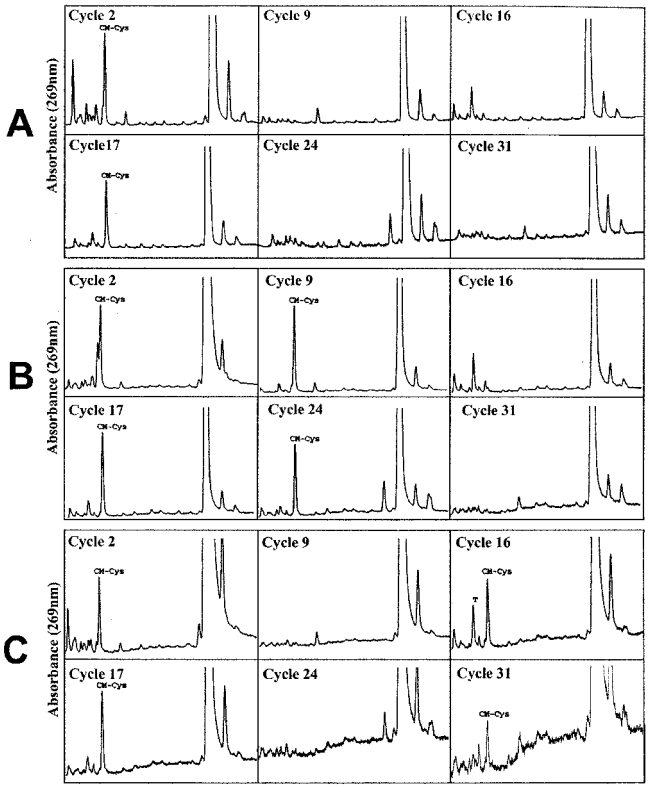

FIG. 3. **HPLC profiles of sequencing partial reduced intermediates after modification with iodoacetamide.** Cysteine residues occur at cycles 2, 9, 16, 17, 24, and 31, indicate on the *left* of the panels. The elution position of Pth-CM-Cys is marked with CM-Cys. *A*, the cysteine residue cycles of alkylated peak 2. *B*, the cysteine residue cycles of alkylated peak 3. *C*, the cysteine residue cycles of alkylated peak 4.

under controlled reducing conditions. Five chromatographic peaks contain intact peptide and partially reduced intermediates, as determined by MALDI-TOF analysis. The main peak (marked *1*) represents intact HWTX-IV, whose observed MALDI mass is the same as the calculated average mass of native HWTX-IV. The mass of peak 2 has 2 Da more in comparison with that of native HWTX-IV, indicating that peak 2 has one of the three disulfide bonds reduced. Peak 3 and peak 4 represent species that are each 4 Da heavier than intact peptide, suggesting two reduced disulfide bonds. Peak 5 represents completely reduced peptide, whose mass is 6 Da heavier than intact HWTX-IV.

Peaks 2–4 were collected and alkalized by adding iodoacetamide before further purification by analytical reverse-phase HPLC. There is 58-Da shift from the original molecular mass after the alkyl group was added to single free thiol upon alkylation. The masses of the three alkalized intermediates determined by MALDI-TOF correspond to the above molecular mass results very well (data not shown).

In Fig. 3*A*, Pth-CM-Cys signal was observed in the chromatograms at the 2nd and 17th cycles after Edman degradation of alkalized peak 1, whereas no Pth-CM-Cys signals were shown at other cysteine cycles. The above result indicates that the only reduced disulfide bond is Cys-2–Cys-17. When sequencing alkalized peak 3, Pth-CM-Cys signals were just observed in the chromatograms at the 2nd, 16th, 17th, and 31st cycles in the HPLC profiles of cysteine cycles (Fig. 3*B*), indicating that Cys-9 is still linked to Cys-24 by a disulfide bond.

For alkalized peak 4, Pth-CM-Cys signals were just observed at the 2nd, 9th, 17th, and 24th sequencing cycles, as showed in Fig. 3*C*. The data indicate that the remaining

HWTX-I	ACKGVFDACTPGKNECCPN- - RVC- SDKHKW- CKWKL
HWTX-IV	ECLEI FKACNPSNDQCCKSSKLVC- SRKTRW- CKYQI*
μ-CTX-GS	ACSGRGSRCOO- - - QCCMG- - LRC- GRGNPQKCI GAHXDV
μ-CTX-GIIIA	RDCCTOOK- KCKDRQCKOQRCCA*
μ-CTX-GIIIB	RDCCTOOR- KCKDRRCKOMKCCA*
μ-CTX-PIIIA	ZRLCCGFOK- SCRSRQCKOHRCC*

FIG. 4. **Comparison of amino acid sequence of HWTX-IV with HWTX-I and previously known conotoxins (*CTX*) blocking at site I (*O* = 4-trans-L-hydroxyproline.** The proposed key residues important for their functions are displayed in the *frame boxes*. Conotoxin GS (38, 39), μ-conotoxin PIIIA (6), μ-conotoxin GIIIA (7, 35, 36), and μ-conotoxin GIIIB (8, 37) block at site I. HWTX-I was suggested to be an *N*-type calcium channel inhibitor (33). Like HWTX-IV and conotoxin GS, it adopts a 1–4, 2–5, 3–6 disulfide pattern and cystine knot motif (32).

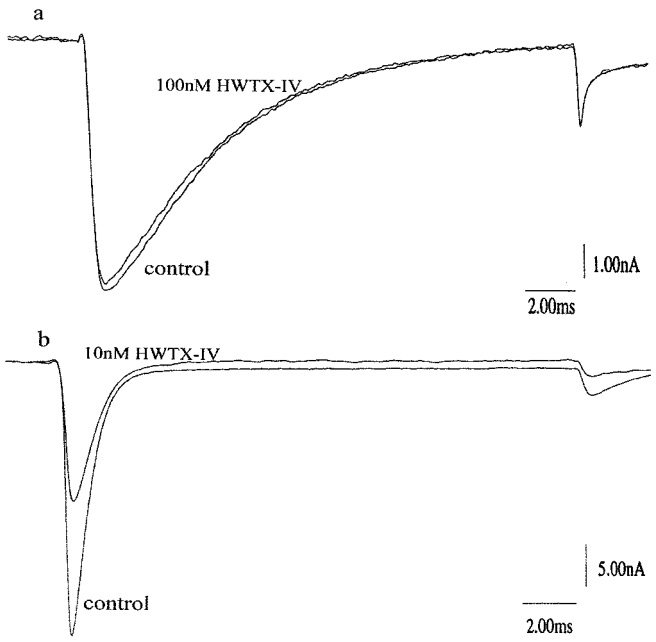

FIG. 5. **Differential effects of HWTX-IV on TTX-R and TTX-S sodium currents.** *a*, TTX-R sodium current was elicited by depolarizing the cell from a holding potential of −80 mV to −10 mV. The duration of the test pulse was 20 ms. 100 nM HWTX-IV did not observably alter the current recorded. *b*, TTX-R sodium current was elicited by depolarizing the cell from a holding potential of −80 mV to −20 mV. The duration of the test pulse was 20 ms. 10 nM HWTX-IV caused a significant decrease in peak current amplitude.

disulfide bond is Cys-16–Cys-31.

All these results indicate that the disulfide linkage of HWTX-IV is Cys-2–Cys-17, Cys-9–Cys-24, and Cys-16–Cys-31, adopting a 1–4, 2–5, 3–6 disulfide pattern. The amino acid sequence of HWTX-IV is shown in Fig. 4.

Effects of HWTX-IV on Sodium Channel Currents—It is widely accepted that two different types of VGSCs exist in rat DRG neurons. TTX-S sodium currents activate and inactivate quickly, whereas TTX-R sodium currents activate and inactivate slowly. TTX at a dose of around 200 nM can suppress TTX-S sodium currents, but TTX-R sodium currents remain almost unchanged at that dose.

When the membrane was held near its resting potential at −80 mV, TTX-S sodium currents were much more sensitive to the blocking action of HWTX-IV than TTX-R currents. HWTX-IV at a dose of 10 nM blocked 15–55% of the TTX-S sodium currents (Figs. 5*a* and 7), whereas TTX-R sodium currents were left intact after the application of HWTX-IV at a concentration up to 100 nM (Fig. 5*b*). The effects of HWTX-IV on the current-voltage relationship are illustrated in Fig. 6. As can be seen from the current-voltage curve, HWTX-IV blocked TTX-S sodium currents to the same degree

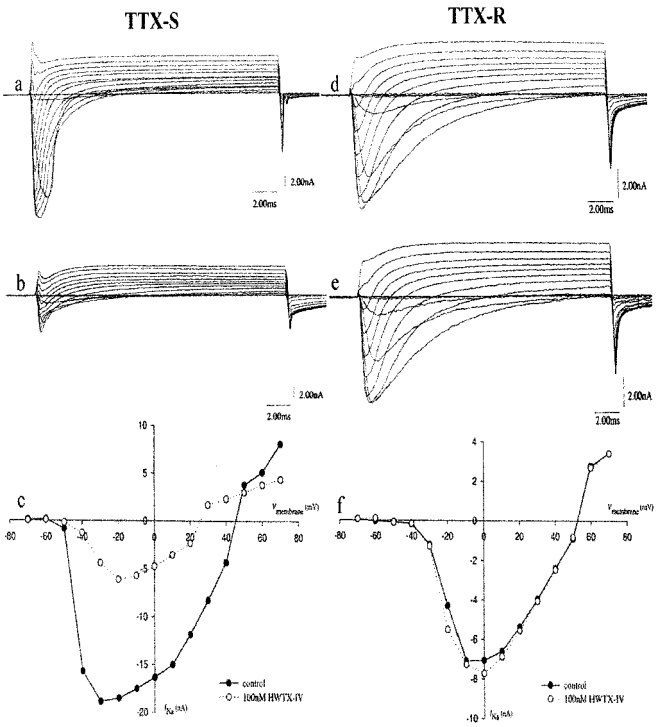

FIG. 6. **Effects of HWTX-IV on I-V relationships of TTX-S and TTX-R sodium currents.** TTX-S (*a* and *b*) and TTX-R (*d* and *e*) sodium currents were recorded before and after the application of 100 nM HWTX-IV. Currents were elicited by 20-ms test pulses from a holding potential of −80 mV to variant potentials from −70 mV to 70 mV with an increment of 10 mV. *c* and *f*, alterations in I-V relationships resulted from the application of HWTX-IV for TTX-S and TTX-R sodium currents, respectively.

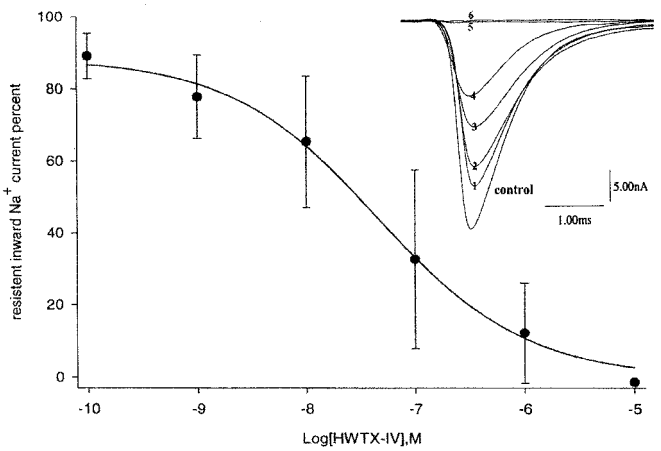

FIG. 7. **Dose-dependent inhibition of HWTX-IV on TTX-S sodium current.** Currents were elicited by 20-ms voltage steps to −20 mV. Cells with a rundown of sodium current above 5% in 3 min were excluded from further statistics. Data points (mean ± S.E., six to eight cells per point) show currents relative to control current amplitudes. The block was determined after toxin had been applied for >1 min. The *inset* shows an illustration of the gradual inhibition of HWTX-IV on peak amplitude of TTX-S current in which *peaks 1–6* represent the effect of HWTX-IV at doses from 0.1 nM to 10 μM with a 10-fold increment.

in the entire membrane potential range (Fig. 6, *a–c*). No significant shift in current-voltage relationship was observed. It seemed that HWTX-IV had no significant effect on TTX-R sodium currents (Fig. 6, *d–f*). The inhibition of HWTX-IV on TTX-S sodium currents was dose-dependent, and the IC_{50} estimated from data collected from six to eight DRG neurons was about 30 nM (Fig. 7), which indicates a

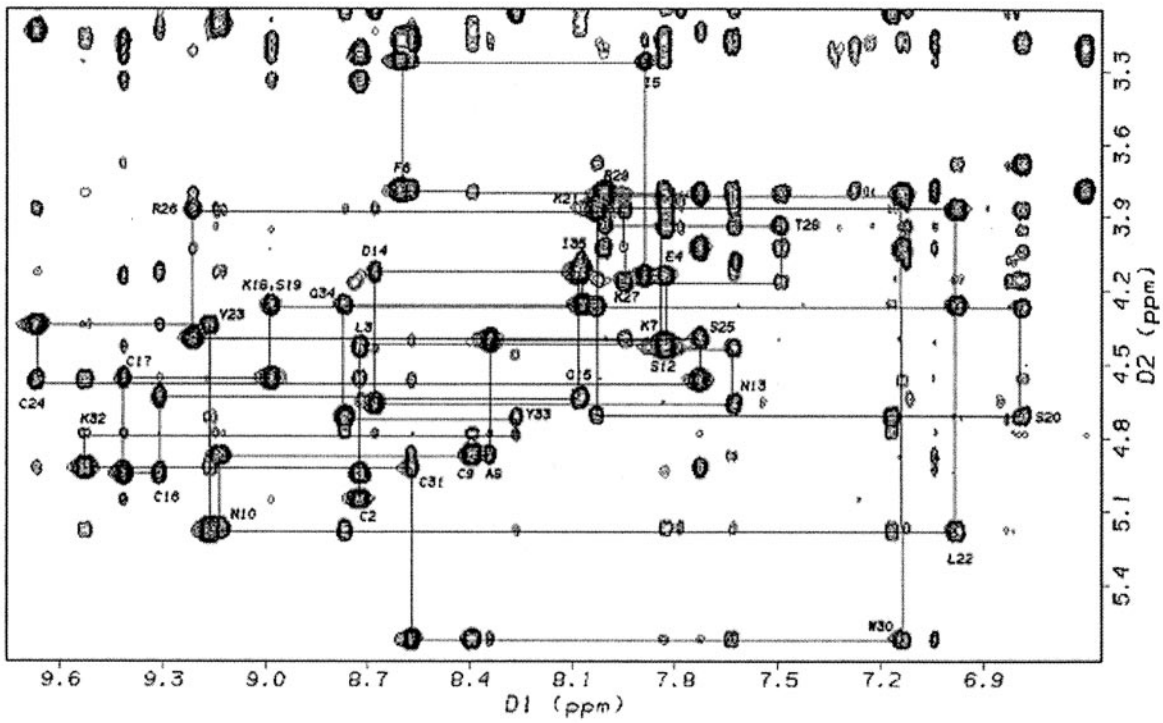

FIG. 8. **Sequential $d_{\alpha N(i,i+1)}$ connectivities in the CαH-NH fingerprint region of the NOESY spectrum.** The mixing time of the NOESY spectrum is 200 ms. Sequential $d_{\alpha N}$ connectivities are shown for residues 1–10 and 12–35. Residue 11 is a proline.

TABLE I
Chemical shifts of the assigned ^{1}H-NMR resonances of HWTX-IV

Residue	NH	C$^\alpha$H	C$^\beta$H	Others
E1		4.175	2.13, 2.15	C$^\gamma$H$_2$ 2.22, 2.45
C2	8.74	5.06	3.25, 3.35	
L3	8.72	4.43	1.42, 1.78	C$^\gamma$H 1.60; C$^\delta$H$_3$ 0.89, 1.00
E4	7.825	4.14	1.82, 2.26	C$^\gamma$H$_2$ 2.32, 2.41
I5	7.89	3.27	1.40	C$^\gamma$H$_2$ 0.06, 0.59; C$^\gamma$H$_3$ 0.74; C$^\delta$H$_3$ 0.31
F6	8.60	3.80	2.94, 3.20	C2, 6 H 6.60; C3, 5H 7.27
K7	7.83	4.42	1.82, 2.15	C$^\gamma$H$_2$ 1.33, 1.61; C$^\delta$H$_2$ 1.71; C$^\varepsilon$H$_2$ 3.04
A8	8.34	4.87	1.57	
C9	8.39	4.88	3.02, 3.12	
N10	9.13	5.18	2.80, 3.04	N$^\delta$H$_2$ 7.13, 7.78
P11		3.95	1.83, 2.10	C$^\gamma$H$_2$ 2.02; C$^\delta$H$_2$ 3.88
S12	7.82	4.44	3.84, 3.95	
N13	7.63	4.67	2.62, 2.69	N$^\delta$H$_2$ 6.85, 7.55
D14	8.67	4.13	2.53, 3.04	
Q15	8.08	4.64	1.80, 2.75	C$^\gamma$H$_2$ 2.36, 2.44; N$^\varepsilon$H$_2$ 6.86, 7.11
C16	9.31	4.95	2.66, 2.76	
C17	9.41	4.56	2.78, 3.19	
K18	8.98	4.26	1.94	C$^\gamma$H$_2$ 1.63; C$^\delta$H$_2$ 1.73; C$^\varepsilon$H$_2$ 3.10
S19	8.99	4.28	3.96, 4.04	
S20	6.78	4.71	3.68, 4.16	
K21	8.03	3.87	2.00, 2.20	C$^\gamma$H$_2$ 1.38; C$^\delta$H$_2$ 1.72; C$^\varepsilon$H$_2$ 3.03
L22	6.97	5.18	0.85, 1.77	C$^\gamma$H 1.44; C$^\delta$H$_3$ 0.35
V23	9.16	4.35	1.89	C$^\gamma$H$_3$ 0.80, 0.88
C24	9.67	4.57	2.56, 3.15	
S25	7.72	4.40	3.81, 4.03	
R26	9.21	3.88	1.85	C$^\gamma$H$_2$ 1.66, 1.77; C$^\delta$H$_2$ 3.23; N$^\varepsilon$H$_2$ 7.45
K27	7.94	4.17	1.75	C$^\gamma$H$_2$ 1.30, 1.42; C$^\delta$H$_2$ 1.64; C$^\varepsilon$H$_2$ 2.96
T28	7.49	3.95	2.56	C$^\gamma$H$_3$ 0.62
R29	8.00	3.81	2.37, 2.06	C$^\gamma$H$_2$ 1.30, 1.45; C$^\delta$H$_2$ 3.24; N$^\varepsilon$H$_2$ 7.33
W30	7.13	5.62	3.20, 2.80	C2H 7.04; C4H 7.63; C5H 7.22 C6H 7.32; C7H 7.60; N1H 10.55
C31	8.57	4.93	3.19, 2.57	
K32	9.53	4.80	1.95	C$^\gamma$H$_2$ 1.45, 1.59; C$^\delta$H$_2$ 1.74; C$^\varepsilon$H$_2$ 3.03
Y33	8.26	4.72	3.07, 2.81	C2, 6H 6.82; C3, 5H 7.17
Q34	8.77	4.25	1.82, 2.20	C$^\gamma$H$_2$ 1.97, 2.24; N$^\varepsilon$H$_2$ 6.88, 7.43
I35	8.07	4.08	1.83	C$^\gamma$H$_2$ 1.21, 1.50; C$^\gamma$H$_3$ 0.95; C$^\delta$H$_3$ 0.94

rather striking potency among all known VGSC antagonists.

Some peptide neurotoxins such as α-scorpion toxins (5) and funnel-web spider toxins (26–28) that interact with a variety of receptor sites on the VGSC can produce repetitive firing of nerves. This symptom is due to toxin-induced alteration in activation and/or inactivation kinetics. Sodium channels are maintained in the open state, and thus the prolonged depolarizing post-potential results in repetitive activity. Unlike these

toxins, HWTX-IV shows no effect on the activation and inactivation kinetics of both TTX-S and TTX-R VGSCs. Its action on TTX-S current is very similar to that of TTX. Thus it is reasonable to take HWTX-IV as a site I toxin, although we have not conducted an isotope-labeled toxin binding assay to test whether it shares the same binding site with TTX.

Sequence-specific Resonance Assignments—The sequence-specific assignment of proton resonances was performed according to standard procedures developed by Wüthrich (23). Spin systems for methyl-containing residues such as Leu-3, Ile-5, Ala-8, Leu-22, Val-23, Thr-28, and Ile-35 were identified through the combined analysis of DQF-COSY, TOCSY, and NOESY spectra. They were used as the start points for the sequential assignment process. The spin system of residue Pro-11 was realized by the observation of strong NOE cross peaks between the α proton of Asn-10 and the δ proton of Pro-11, which also suggests that residue Pro-11 in HWTX-IV takes the trans configuration. All backbone and more than 95% of side chain proton resonances belonging to spin systems for each of the 35 amino acid residues were assigned. Fig. 8 shows the sequential $d_{\alpha N(i,i+1)}$ connectivities on the CαH-NH fingerprint region of the NOESY spectrum with a mixing time of 200 ms. Table I shows the summary of the chemical shifts of proton resonances of HWTX-IV.

Structure Calculation and Evaluation—527 irredundant distance constraints derived from NOEs and 14 dihedral constraints derived from $^3J_{HN\alpha}$ coupling constants had been used to calculate the structure of HWTX-IV by distance geometry and simulated annealing calculation with the program XPLOR. The initial structures were refined by two rounds of simulated annealing with force constants 50 kcal mol^{-1} Å^{-2} and 200 kcal mol^{-1} rad^{-2} for NOE distance and dihedral angel constraints, respectively. An ensemble of 20 structures with lower energy and better Ramachandran plots were chosen to represent the three-dimensional solution fold of HWTX-IV. NOE violations of all of these 20 structures are less than 0.3 Å, and dihedral violations are less than 2 degrees. The 20 structures exhibit no significant deviation from ideal covalent geometry, satisfy the experiment constraints with minimal violations, and have good non-bonded contacts as evidenced by the low values of the mean Lennard-Jones potential. Structural statistics are shown in Table II. Analysis of the family of 20 structures using the program PROCHECK (29) reveals that 81.6% of all the non-Pro/Gly residues lie in the most favored regions of the Ramachandran plot, and the remaining 18.4% lie in the additionally allowed regions. The 20 structures converged to a common fold; the root mean square differences (R.M.S.D.) of 20 structures (pairwise comparison or *versus* mean structure) are low (Table II).

The coordinates for the family of 20 structures and NMR constraints file have been deposited in the Brookhaven Protein Data Bank (PDB) with accession code 1MB6. The ^{1}H chemical shifts have been deposited in BioMagResBank (BMRB) with accession code RCSB016799.

Three-dimensional Structure of HWTX-IV—Fig. 9*A* shows a stereo pair representation of the best-fit superposition of the Cα trace for the 20 structures of HWTX-IV. The trace is colored from blue to white according to increasing R.M.S.D. Analysis of the ensemble of 20 structures indicates that a main structural characteristic of HWTX-IV is a double-stranded antiparallel β-sheet (Fig. 9*B*), which is formed by the strands Leu-22–Ser-25 and Trp-30–Tyr-33, respectively. The information from the large $^3J_{HNH\alpha}$ coupling constants, chemical shift index (CSI), slowly exchanging amide protons, strong sequential $d_{\alpha N}$ and weak d_{NN}, as well as interstrand NOE connectivities also occurs with such a β-sheet. Turns in HWTX-IV have been identified by the standard that the distance between Cα(i) and Cα(i+3) is less that 7 E and classified according to Richardson (30). Four β-turns have been found in the structure of HWTX-IV, as shown in Table III and Fig. 9*B*. β-turns 11–14, 17–20, and 26–29 are type I, and turn 4–7 is type II.

TABLE II
Structural statistics for the family of 20 structures of HWTX-IV

Experimental constraints	Number
Intra-residue NOE (i − j = 0)	122
Sequential NOE (|i − j| = 1)	162
Medium range NOE (|i − j| ≤ 5)	75
Long range NOE (|i − j| ≥ 5)	168
Dihedral angle (ϕ)	14
r.m.s. deviation from experimental constraints[a]	
NOE distance (Å) (527)	0.003 ± 0.001
Dihedral angle (deg.) (16)	0.112 ± 0.06
r.m.s. deviations from idealized geometry[b]	
Bonds (Å)	0.003 ± 0.0001
Angles (deg)	0.552 ± 0.009
Impropers (deg)	0.351 ± 0.006
Mean energies (kcal mol^{-1})[b]	
E_{bond}	6.564 ± 0.505
E_{angle}	47.975 ± 1.494
$E_{improper}$	5.454 ± 0.197
E_{vdW}	−96.848 ± 6.351
E_{NOE}	0.294 ± 0.191
E_{cdih}	0.006 ± 0.014
E_{total}	−36.556 ± 7.792
Average r.m.s. differences versus mean structure (Å)	
Backbone atoms (N, Cα, C)	0.389 ± 0.077
Non-hydrogen heavy atoms	1.106 ± 0.141
Average pairwise r.m.s. differences (Å)	
Backbone atoms (N, Cα, C)	0.615 ± 0.112
Non-hydrogen heavy atoms	1.587 ± 0.160

[a] The statistics of experimental R.m.s. deviation of NOE and dihedral angle constraints were from the calculation with force constants of 50 kcal mol^{-1} Å^{-2} and 200 kcal mol^{-1} rad^{-2}, respectively.

[b] The idealized geometry and energy values were defined by the CHARMM force field as implemented in the XPLOR program. All statistical values of energies, R.m.s. deviations, and R.m.s. differences are given as the mean ± S.D.

HWTX-IV adopts an ICK motif commonly observed in toxic and inhibitory polypeptides (17, 31). In HWTX-IV, the cystine knot is formed by three disulfide bonds linking as Cys-2–Cys-17, Cys-9–Cys-24, and Cys-16–Cys-31 in which the disulfide Cys-16–Cys-31 passes through a 16-residue ring formed by the other two disulfide bridges (Cys-2–Cys-17 and Cys-9–Cys-24) and the intervening polypeptide backbone. The amino acid sequence of the ICK fold in HWTX-IV can be written as CX_6CX_6CCX_6CX_6C, where *X* is any amino acid residue. Structural comparison shows that the R.M.S.D. between HWTX-IV and huwentoxin-I (HWTX-I) (Fig. 9*C*), a toxin purified from the same spider venom that also adopts the ICK fold but shows inhibition on N-type Ca^{2+} channel current (33), is 1.31 Å for trace Cα atoms. It indicated that the three-dimensional structures of HWTX-IV and HWTX-I (Protein Data Bank code: 1QK6) are highly similar although their biological functions are completely different.

DISCUSSION

The Target of HWTX-IV—Several potent toxins target voltage-gated sodium channels; the different sites of binding and modes of activity of these toxins are very significant for investigating the structure and function of these sodium channels, which play a key role in excitable tissues. TTX, an extensively investigated non-peptide sodium channel blocker, targets a site

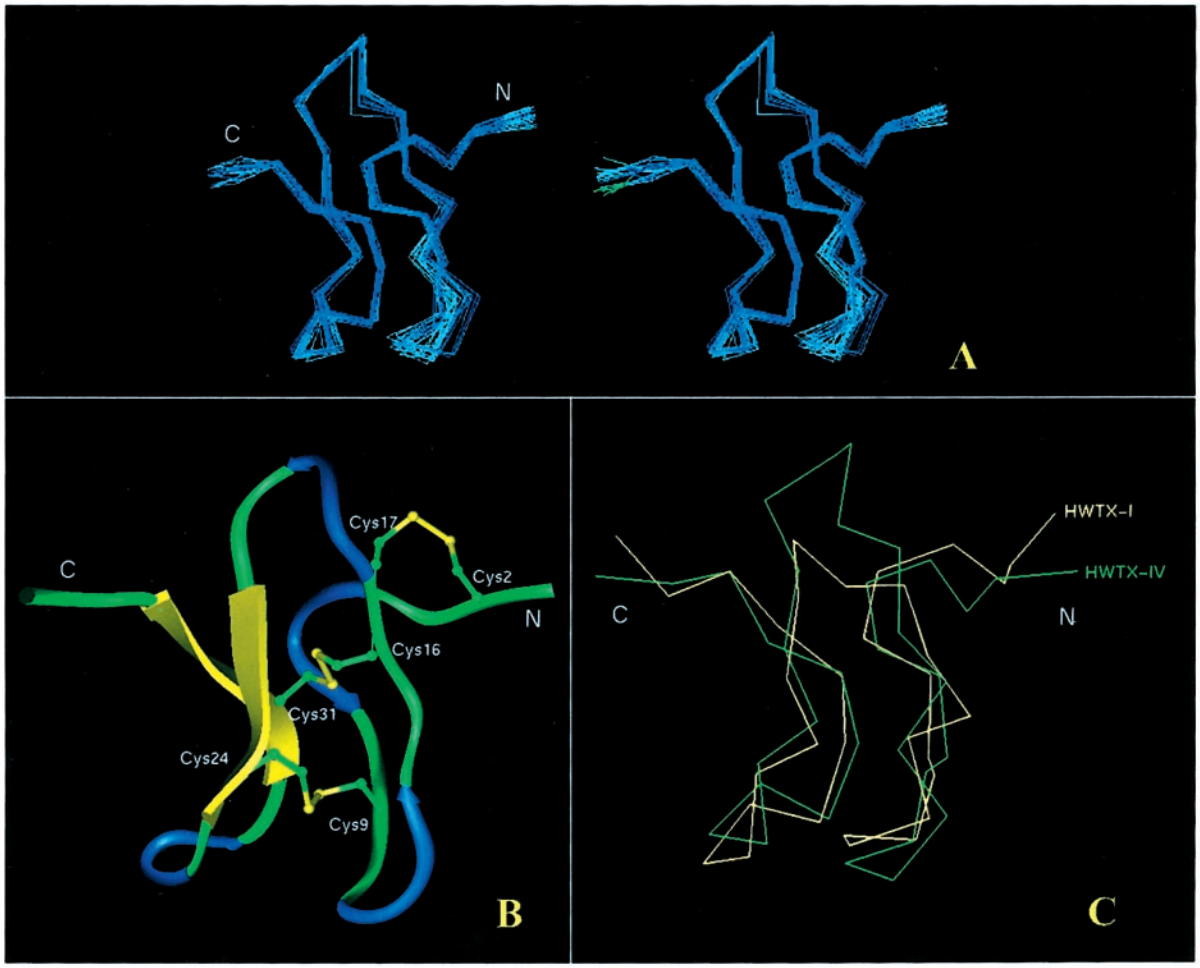

FIG. 9. **Solution structure characterization of HWTX-IV.** *A*, stereo view of superimposition of Cα atoms for the ensemble of 20 structures. The *color* of the traces is brightened from *blue* to *white* according to the increasing of R.M.S.D. *B*, the schematic of HWTX-IV illustrates the location of secondary structures. The β-sheet is shown in *yellow*, turns are shown in *blue*, and the random coil structure is shown in *green*. Three disulfide bonds (Cys-2–Cys-17, Cys-9–Cys-24, and Cys-16–Cys-31) are indicated. *C*, comparison of HWTX-IV and HWTX-I (Protein Data Bank code: 1QK6). The Cα trace of HWTX-IV is shown in *green*, and the Cα trace of HWTX-I in shown in *yellow*.

TABLE III
Four μ-turns in the structure of HWTX-IV

Number	Loop	$d_{C\pm(i,i+3)}$	ϕ	ψ	ϕ	ψ	Type
		Å	°	°	°	°	
1	4–7	5.75	−65.4	152.3	57.0	36.8	II
2	11–14	5.83	−76.6	−35.9	−112.5	79.7	I
3	17–20	5.82	−74.2	−25.1	−59.8	−34.8	I
4	26–29	4.68	−63.0	−42.3	−88.5	−14.4	I

generally postulated to be at the extracellular end of the channel pore (site I). HWTX-IV shows no effect on the activation and inactivation kinetics of both TTX-S and TTX-R VGSCs, and its action on TTX-S current is very similar to that of TTX. Thus it is reasonable to consider HWTX-IV as a site I toxin, although we have not conducted an isotope-labeled toxin binding assay to test whether it shares the same binding site with TTX. So far only one family of polypeptide toxins, the μ-conotoxins from *Conus*, has been shown to act at this site and functionally affect voltage-gated sodium currents. The amino acid sequence of HWTX-IV is quite different from that of μ-conotoxins, so it should prove to be a novel useful ligand to investigate the multiple molecular forms of voltage-gated sodium channels.

Structure-Activity Relationship of HWTX-IV—Many research groups have demonstrated that negatively charged residues of the sodium channel are important in the binding of site I toxins to their targets, and guanidinium groups in these toxins are of particular importance for their actions on the sodium channel (6–8, 34–37). Studies of μ-conotoxin GIIIA suggested that the largest activity loss was introduced when Arg-13 or Arg-19 was replaced (36). Conotoxin GS binds competitively with μ-conotoxin GIIIA to the sodium channel surface (site I), but these two conotoxins have little sequence and structure identity with one other (38, 39). Unlike μ-conotoxins, both conotoxin GS and HNTX-IV adopt a cystine-knot motif with the same disulfide bond pattern. Loop 4 of HWTX-IV looks like a flexible segment, and almost no long distance or medium distance NOE constraint correlating with other sections of the toxin could be observed in its NMR spectra. The sequence alignment of these two toxins shows that Arg-26, which is located in the flexible loop 4 of HWTX-IV, is conserved. Like all toxins that block at site I, the guanidinium group of Arg is supposed to be critical to the function of HWTX-IV.

Biological Implication of HWTX-IV—HWTX-IV at a dose as high as 200 $\mu g\ g^{-1}$ showed no effect in the adult American cockroach. Nor does it target VGSCs in cardiac or skeletal muscle of both amphibians and mammals. It selectively inhibits neuronal TTX-S VGSC in mammals, acting most likely as a site I antagonist. Such a specificity is still unavailable from any other peptide toxin so far known. Characterization of HWTX-IV and investigation of its interaction with VGSCs are sure to provide us with insight into the gating mechanism of neuronal sodium channels as well as the different roles of

diverse sodium channels in signal integration in the nervous system.

Both TTX-S VGSCs and TTX-R VGSCs in DRG neurons are involved in the pain pathway. However, for different kinds of pain symptoms, their involvements seem to be of variant degrees. Furthermore, the delicate cooperation between these two subtypes might be of equal importance to that pathway as well (25). Now that HWTX-IV selectively blocks the TTX-S sodium current in DRG neurons, it is hoped that it can be applied in pain therapy. Actually, judged by our preliminary experiments, it does introduce a significant upgrade to the pain threshold in rats (data not shown).

In summary, we have found a highly potent neurotoxin, huwentoxin-IV, that specifically inhibits the neuronal tetrodotoxin-sensitive voltage-gated sodium channel. This toxin seems to be a site I toxin, like μ-conotoxins (6–8, 36, 37), affecting the sodium channel through a mechanism quite similar to that of TTX. The three-dimensional structure of HWTX-IV determined by two-dimensional ^{1}H NMR proved that the molecule adapted a typical ICK motif. It should prove to be a novel ligand useful to investigate the multiple molecular forms of voltage-gated sodium channels.

Acknowledgments—We thank Dr. Jihui Wu (University of Science and Technology of China) for collecting two-dimensional NMR spectra and Weijun Hu (Hunan Normal University) for the peptide sequence analysis. We are grateful to Prof. Jinyung Xie (Hunan Normal University) and Dr. Shanyun Lu (Peking University) for the helpful discussions.

REFERENCES

1. Narahashi, T., Deguchi, T., Urakama, N., and Ohkubo, Y. (1960) *Am. J. Physiol.* **198,** 934–938
2. Narahashi, T., Moore, J. W., and Scott, W. R. (1964) *J. Gen. Physiol.* **47,** 965–974
3. Roy, M. L., and Narahashi, T. (1992) *J. Neurosci.* **12,** 2104–2111
4. Strachan, L. S., Lewis, R. J., and Nicholson, G. M. (1998) *J. Pharmacol. Exp. Ther.* **288,** 379–388
5. Possani, L. D., Becerril, B., Delepierre, M., and Tytgat, J. (1999) *Eur. J. Biochem.* **264,** 287–300
6. Shon, K. J., Oliver, M. B., Watkins, M., Jacobsen, R. B., Gray, W. R., Floresca, C. Z., Cruz, L. J., Hillyard, D. R., Brink, A., Terlau, H., and Yoshikami, D. (1998) *J. Neurosci.* **18,** 4473–4481
7. Chahine, M., Sirois, J., Marcotte, P., Chen, L. Q., and Kallen, R. G. (1998) *Biophys. J.* **75,** 236–246
8. Li, R. A., Ennis, I. L., Vélez, P., Tomaselli, G. F., and Marbàn, E. (2000) *J. Biol. Chem.* **275,** 27551–27558
9. Meir, A., Ginsburg, S., Butkevich, A., Kachalsky, S. G, Kaiserman, I., Ahdut, R., Demirgoren, S., and Rahamimoff, R. (1999) *Physiol. Rev.* **79,** 1019–1087
10. Sampo, B., Tricaud, N., Leveque, C., Seagar, M., Couraud, F., and Dargent, B. (2000) *Proc. Natl. Acad. Sci. U. S. A.* **97,** 3666–3671
11. Boccaccio, A., Moran, O., Irnoto, K., Conti, F. (1999) *Biophys. J.* **77,** 229–240
12. Penzotti, J. L., Fozzard, H. A., Lipkind, G. M., and Dudley, S. C. (1998) *Biophys. J.* **75,** 2647–2657
13. Hilber, K., Sandtner, W., Kudlacek, O., Glaaser, I. W., Weisz, E., Kyle, J. W., French, R. J., Fozzard, H. A., Dudley, S. C., and Todt, H. (2001) *J. Biol. Chem.* **276,** 27831–27839
14. Waxman, S. G., Dib-Hajj, S., Cummins, T. R., and Black, J. A. (1999) *Proc. Natl. Acad. Sci. U. S. A.* **96,** 7635–7639
15. Porreca, F., Lai, J., Bian, D., Wegert, S., Ossipov, M. H., Eglen, R. M., Kassotakis, L., Novakovic, S., Rabert, D. K., Sangameswaran, L., and Hunter, J. C. (1999) *Proc. Natl. Acad. Sci. U. S. A.* **96,** 7640–7644
16. Cummins, T. R., and Waxman, S. G. (1997) *J. Neurosci.* **17,** 3503–3514
17. Pallaghy, P. K., Nielsen, K. J., Craik, D. J., and Norton, R. S. (1994) *Protein Sci.* **3,** 1833–1839
18. Shu, Q., and Liang, S. (1999) *J. Pept. Res.* **53,** 486–491
19. Wu, J., and Watson, J. T. (1997) *Protein Sci.* **6,** 391–398
20. Gray, W. R. (1993) *Protein Sci.* **2,** 1732–1748
21. Gray, W. R. (1993) *Protein Sci.*, **2,** 1749–1755
22. Hu, H. Z., and Li, Z. W. (1997) *J. Physiol.* **501,** 67–75
23. Wüthrich, K. (1986) *NMR of Proteins and Nucleic Acids*, John Wiley & Sons, Inc., New York
24. Brünger, A. T. (1992) *X-PLOR Manual, Version 3.1.*, Yale University, New Haven, CT
25. Waxman, S. G. (1999) *Pain* **6,** (suppl.) S133–S140
26. Nicholson, G. M., Willow, M., Howden, M. E. H., and Narahashi, T. (1994) *Eur. J. Physiol.* **428,** 400–409
27. Nicholson, G. M., Little, M. J., Tyler, M., and Narahashi, T. (1996) *Toxicon* **34,** 1443–1453
28. Nicholson, G. M., Walsh, R., Little, M. J., and Tyler, M. (1998) *Eur. J. Physiol.* **436,** 117–126
29. Laskowski, R. A., MacArthur, M. W., Moss, D. S., and Thornton, J. M. (1993) *J. Appl. Cryst.* **26,** 283–291
30. Richardson, J. S. (1981) *Adv. Protein Chem.* **34,** 167–236
31. Norton, R. S., and Pallaghy, P. K. (1998) *Toxicon* **36,** 1573–1583
32. Zhang, D., and Liang, S. (1993) *J. Protein Chem.* **12,** 735–740
33. Peng, K., Chen X., and Liang S. (2001) *Toxicon* **39,** 491–498
34. Rogers, J. C., Qu, Y. S., Tanada, T. N., Scheuer, T., and Catterall, W. A. (1996) *J. Biol. Chem.* **271,** 15950–15962
35. Li, R. A., Ennis, I. L., French, R. J., Dudley, S. C., Jr., Tomaselli, G. F., and Marbàn, E. (2001) *J. Biol. Chem.* **276,** 11072–11077
36. Sato, K., Ishida, Y., Wakamatsu, K., Kato, R., Honda, H., Ohizumi, Y., Nakamura, H., Ohya, M., Lancelin, J. M., Kohda, D., and Inagaki, F. (1991) *J. Biol. Chem.* **266,** 16989–16991
37. Hill, J. M., Alewood, P. F., and Craik, D. J. (1996) *Biochemistry* **35,** 8824–8835
38. Hill, J. M., Alewood, P. F., and Craik, D. J. (1997) *Structure* **5,** 571–583
39. Yanagawa, Y., Abe, T., Satake, M., Odani, S., Suzuki, J., and Ishikawa K. (1988) *Biochemistry* **27,** 6256–6262